

Heuristical and numerical considerations for the carbuncle phenomenon

Friedemann Kemm

March 7, 2017

Keywords: Carbuncle phenomenon, High speed flow, Shock instability, High resolution schemes, Riemann solver

MSC 2010: 76J20, 76K05, 76L05, 76M99, 76N15

In this study, we investigate the so called carbuncle phenomenon by means of numerical experiments and heuristic considerations. We identify two main sources for the carbuncle: instability of the 1d shock position and low numerical viscosity on shear waves. We also describe how higher order stabilizes the 1d shock position and, thus, reduces the carbuncle.

1 Introduction

For the simulation of shock structures in multidimensional gas flows there are essentially two major approaches: shock fitting and shock capturing. The idea of the first class of schemes is to exactly detect the shock position and split the computational domain along the shock line into two (or for more complex structures even more) domains, leading to an almost perfect reproduction of shocks in the numerical solution [11, 41, 42]. Disadvantages of this method include the difficulty to deal with shocks which unexpectedly evolve in the domain and a practical restriction to certain shock structures. In order to overcome these restrictions, more and more scientists started to build their simulations on shock capturing schemes, which are designed to work without the knowledge of the exact shock position. Thus, the shock is captured in a (hopefully) thin layer of grid cells. For an overview over shock fitting schemes and some recent developments in that area, we refer to [6, 52].

A main ingredient of shock capturing schemes are so called Riemann solvers: numerical (first order) flux functions, which are based on an approximate solution of the Riemann problem at the cell face. This class was later on expanded, starting with [54, 56], through introduction of Flux-Vector-Splitting schemes, which are based on a splitting of the physical flux function, but in a wider sense can be considered as Riemann solvers. More important for our study however, is the distinction between complete and incomplete Riemann solvers. While the first are designed to resolve all waves present in a Riemann problem, the latter will neglect some waves. Prominent examples of complete Riemann solvers are the schemes by Roe [50] and Osher [44]. While these solvers are preferable when complex wave structures as well as entropy and shear waves are expected, incomplete solvers are known to be robust in situations dominated by strong shocks. An example is the HLL-solver [21] whose construction is based only on the two outer waves of the Riemann problem. In the eighties and nineties, more and more applications were treated with above mentioned methods for gas dynamics. The methods were also extended to other hyperbolic conservation laws like shallow water or compressible magnetohydrodynamics (MHD). For a detailed discussion of shock capturing, we refer to the textbooks [16, 17, 35–37, 58, 61].

In the context of shock capturing, some irregularities were observed: properties of the discrete solutions which were by no means representations of physical phenomena. In gas dynamics simulations unphysical discrete shock structures and even a complete breakdown of the discrete shock profile could appear [47, 48]. According to its form in blunt body problems, it was christened *carbuncle phenomenon*. Since the seminal paper of Quirk [48], an immense amount of research has been conducted on this instability problem. The origin of the name comes from the fact that in strongly supersonic flows against an infinite cylinder simulated on a body-fitted, structured mesh the middle part of the resulting bow shock degenerates to a carbuncle-shaped structure. It was conjectured already by Quirk [48] that this phenomenon is closely related to other instabilities such as the so-called *odd-even-decoupling* encountered in straight shocks aligned with the grid. Unfortunately, the failure is only found in schemes with high resolution of shear and entropy waves, so called complete Riemann solvers, which are needed to properly resolve the boundary layers and turbulent structures. This category includes for example the Godunov, Roe, Osher, HLLC and HLLM schemes [13, 58]. These schemes are preferable in calculations involving complex wave structures as well as boundary layers.

The research on the carbuncle was twofold. On the one hand, the stability of discrete shock profiles was investigated in one as well as in several space dimensions. On the other hand, a lot of effort was put into finding cures for the failure of some schemes in numerical calculations. For example, many cures that were offered, are based on an indicator that tells the scheme when to switch to an incomplete Riemann solver. These indicators need information from other cell faces, making the numerical flux function non-local. It was found that even in one space dimension there are some instabilities of discrete shock profiles: slowly moving shocks produce small post-shock oscillations [1, 23, 48]. But also in the case of a steady shock, instabilities can be found depending on the value of the

adiabatic coefficient γ as was shown by Bultelle et al. [7]. However, the connection to two-dimensional instabilities is still not fully understood.

The two-dimensional instabilities themselves seem to be closely related to each other. Chauvat et al. [9] show through an ingenious numerical investigation that the mechanisms driving the odd-even-decoupling and the carbuncle are closely related. Dumbser et al. [12] present a method to test Riemann solvers for their tendency to odd-even-decoupling. Here, the basic idea is to discretise a steady shock in space and test the linear stability of the system of ODEs resulting from the Method of Lines. This allows for all tested solvers to predict whether they would evolve an instability or not. There is also a number of experimental studies of the carbuncle, especially the influence of the underlying numerical flux function [32–34, 59], with the goal to identify the “optimal Riemann solver”. Finally, Elling [14] found a connection to physical shock instabilities.

Most these investigations have in common that they (a) intend to find a single source for the carbuncle, (b) do not take into account the influence of the order of the scheme—they usually compare different Riemann solvers in a scheme with fixed order—, and (c) do not distinguish between the contribution of entropy or shear waves to the carbuncle. The most surprising is case (b) since it is well known that in higher order schemes the carbuncle is much weaker than in first order; for very high orders, it is essentially absent. The purpose of this paper is to fill these gaps in research. We want to study the influence of the (1d) stability of the shock position and the 2d or 3d features such as vorticity separately. In this course, we also try to separate the influences of entropy and shear waves. But the main focus (and main novelty) of this study is that we investigate the influence of the order of the scheme on the stability of the (1d) shock position. We will show how increasing the order of the scheme, despite of lowering the numerical shear viscosity, stabilizes the 1d shock position.

The outline of the paper is as follows: In Section 2 we give a short representative review of some theoretical results. The insight gained by these results provides us with the guidelines for our numerical experiments. In Section 3, we give a review of the schemes we use in our numerical experiments. The numerical test cases are introduced in Section 4. The main results are presented in Sections 5 (one-dimensional issues) and 6 (multi-dimensional issues), followed by some conclusions and directions for further research in Section 7.

2 Short review of the theory

There are many papers dedicated to the carbuncle phenomenon [1, 3, 7, 9, 14, 29, 31, 43, 45, 46, 48, 53, 63–65], however only few of them discuss the origins of the carbuncle from a theoretical point of view. Here, we give a short representative review of some theoretical results.

2.1 Contribution by Bultelle et al.

Bultelle et al. [7] investigate steady shocks in one space dimension. A first study of these was done by Barth [4] who found that for a perfect gas with $\gamma = 1.4$, flux functions which enforce the Rankine-Hugoniot condition at discontinuities may have transition states which are unstable to perturbations when the preshock Mach number is greater than six. Bultelle et al. go even further. They prove that the Godunov scheme for strong steady shocks and an adiabatic coefficient $1 \leq \gamma^* \approx 1.62673$, with γ^* being a root of

$$\gamma^4 + 3\gamma^3 - 21\gamma^2 + 17\gamma + 8 = 0,$$

can produce unstable shock profiles. They report that in practice, after a transient regime, the unstable leads to a stable profile with the intermediate state in a neighbouring cell or even one cell further. If in neighbouring grid slices normal to the shock front, the shock position jumps in a different direction, say +2 cells in one and -2 cells in another slice, this leads to an unphysical crossflow along the shock. We discuss this situation in more detail in Section 5.1.

2.2 Contribution by Roe and Zaide

While Bultelle et al [7] discuss steady shocks in general, Roe and Zaide [63–65] focus on the long-time behavior. Although they mainly discuss the standard Roe solver, the discussion relies on the fact that the solver tries to establish the exact Rankine-Hugoniot condition at single shocks. Thus, we can expect that their results also apply to other Riemann solvers with this property, e. g. Godunov, HLLE etc. Roe and Zaide investigate the behavior of steady discrete shocks with one intermediate point in 1d. For the Euler equations (and also for the shallow water equations) it is impossible to find for a non-trivial steady shock with left and right states \mathbf{q}_l and \mathbf{q}_r , which are related via the Rankine-Hugoniot condition, a middle state \mathbf{q}_m which is related to both states via the same condition. As a result, the scheme enforces a middle state which is unphysical. In some situations, \mathbf{q}_m is not even constant in time: the shock, although unsteady, is trapped in a single grid cell. And even if \mathbf{q}_m is steady, the shock position in the cell is ambiguous. Depending on the conservative variable used to compute the shock position one gets different results. Another feature of these shocks is an overshoot in the momentum, which is also the mass flux, again indicating the deviation of the discrete solution from real world physics.

From these results we can draw the conclusion that, at least for Riemann solvers based on the Rankine-Hugoniot condition, even shocks which remain in the same grid cell are highly sensitive to perturbations.

2.3 Contribution by Elling

Elling [14] investigates the influence of the supersonic upstream region on the shock profile. He models the interaction of a vortex filament with a strong shock. For this purpose,

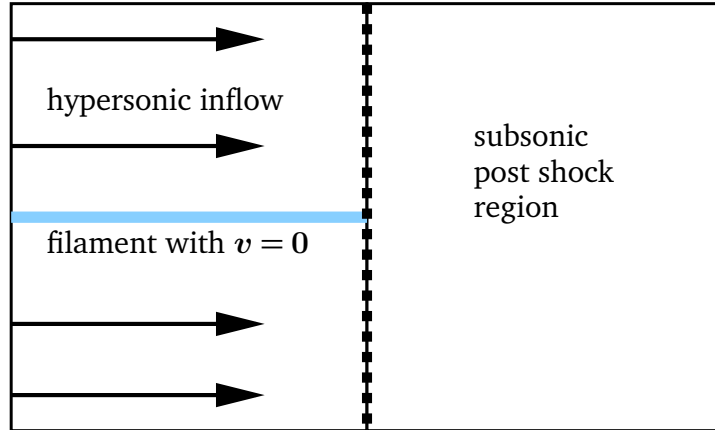


Figure 1: Model situation for physical carbuncle.

he starts with a steady shock. In the region upstream of the shock, he picks the middle slice of the computational grid and artificially sets the velocity to zero as sketched out in Figure 1. This closely corresponds to the experimental and theoretical investigations by Kalkhoran and Smart [24] and by Zhang et al. [66]. It turns out that the carbuncle-like structure which comes with the Godunov-scheme is similar to the experimental results. Furthermore, Elling gives numerical evidence that the structure does not depend on the energy inherent in the filament. Even more so, the structure is the same for all reasonable resolutions of the computational domain. The numerical results obtained with Osher or HLLEM are almost identical to those obtained with the Godunov scheme in contrast to the HLLE and other incomplete Riemann solvers. We find that in real world simulations of a shock interacting with a vortex filament, the viscosity, especially the shear viscosity, of HLLE and other incomplete Riemann solvers is too high. It outweighs the physical viscosity by far. This explains why Elling not only states that the carbuncle is incurable but also that the carbuncle should not (completely) be cured, or better: not completely be prevented. The challenge is to avoid unphysical carbuncles and, at the same time, allow physical carbuncles. In other words, one has to look for schemes which allow shear and entropy waves to be well resolved but still prevent the unphysical breakdown of shock waves.

3 Review of the numerical schemes for our experiments

In order to perform meaningful numerical experiments, one has to choose a suitable set of numerical methods. Since it is well known that the choice of the Riemann solver has a strong impact on the tendency of the scheme to develop a carbuncle, we have to compare Riemann solvers which differ from each other in some features coincide in other features. Motivated by the discussion in the previous section, we choose solvers with different approaches at

shocks: Osher as an example of a solver which abandons the Rankine-Hugoniot condition as a construction principle and some members of the Roe/HLL-family which in general force the Rankine-Hugoniot condition at single shocks¹. Since the carbuncle is characterized by strong shear flows among the Roe/HLL-type solvers, we select HLLEM, HLLEMCC, and HLLC in order to compare different shear viscosity mechanisms and their relation to the carbuncle. For the discussion of the influence of the order of the scheme on the carbuncle, we employ several standard 1st- and 2nd-order variants as described below.

3.1 Basic finite volume scheme

For shallow water equations, we employ CLAWPACK [10], which is an implementation of the wave propagation approach. Thus, limiting for higher order is always done on characteristic variables. Higher order calculations are done (1) on Cartesian grids with the Superpower limiter [26, 27] and (2) on non-Cartesian grids with the Albada 3 limiter [26]. Both are smooth limiters. While on Cartesian grids the more compressive Superpower limiter could be applied, on non-Cartesian grids one has to go back to a less compressive limiter. In Section 17 we will discuss the reason why it is advantageous to opt for a more compressive limiter. The Superpower limiter is a generalization of the Power limiter by Serna and Marquina [55]. In contrast to the original Power limiter, the powers are not fixed but adapted to the local CFL-number in such a manner that the resulting limiter is always TVD and approaches third order behavior in smooth regions. The Albada p limiters are derived from the van-Albada limiter in the same way as Serna and Marquina derived the Power limiters from the van Leer limiter. While Power 2 is just the original van Leer limiter, Albada 2 is just the original van Albada limiter. Albada 3 is the most compressive version that still makes up a CFL-number independent TVD limiter.

For the Euler results, we employed Euler2d, a 2d-Cartesian code developed in the Group of Claus-Dieter Munz at Stuttgart University. The code implements standard finite volumes. For higher order, direction-wise geometric limiting with minmod on primitive variables is used.

3.2 Roe, HLL and their relatives

Since the Roe scheme and the HLL-type schemes are closely related [13, 28], we treat them as one family of schemes. For a better understanding it is convenient to start with the Roe scheme.

3.2.1 Roe

The core of the Roe scheme is a consistent local linearization [50], which was first announced by Roe and Baines [51] as a means to employ their TVD-limiters in a wave-wise manner. In

¹We will also present a modification of HLLEM that yields a behavior at steady shocks close to the Osher scheme.

the linear case, one finds for the flux function

$$f(\mathbf{q}) = \mathbf{A} \mathbf{q} \quad (1)$$

and, thus, for the flux difference

$$f(\mathbf{q}_r) - f(\mathbf{q}_l) = \mathbf{A}(\mathbf{q}_r - \mathbf{q}_l). \quad (2)$$

For a local linearization to ensure local conservation, it is crucial to satisfy a similar condition. Furthermore, the linearized system should be hyperbolic, and the system matrix should depend continuously on the left and right states \mathbf{q}_l and \mathbf{q}_r . Therefore, Roe came up with the following conditions for a consistent linearization with system matrix $\tilde{\mathbf{A}}(\mathbf{q}_l, \mathbf{q}_r)$:

$$f(\mathbf{q}_r) - f(\mathbf{q}_l) = \tilde{\mathbf{A}}(\mathbf{q}_l, \mathbf{q}_r)(\mathbf{q}_r - \mathbf{q}_l), \quad (3)$$

$$\tilde{\mathbf{A}}(\mathbf{q}_l, \mathbf{q}_r) \rightarrow \mathbf{A}(\mathbf{q}) \quad \text{for} \quad (\mathbf{q}_l, \mathbf{q}_r) \rightarrow (\mathbf{q}, \mathbf{q}), \quad (4)$$

$$\tilde{\mathbf{A}}(\mathbf{q}_l, \mathbf{q}_r) \text{ is diagonalizable for all } \mathbf{q}_l, \mathbf{q}_r. \quad (5)$$

A matrix $\tilde{\mathbf{A}}(\mathbf{q}_l, \mathbf{q}_r)$ that satisfies these conditions is called a Roe matrix or a consistent local linearization for the underlying system of conservation laws. If there exists a single state $\tilde{\mathbf{q}} = \tilde{\mathbf{q}}(\mathbf{q}_l, \mathbf{q}_r)$ with

$$\tilde{\mathbf{A}}(\mathbf{q}_l, \mathbf{q}_r) = \mathbf{A}(\tilde{\mathbf{q}}), \quad (6)$$

then it is called a Roe mean value for $\mathbf{q}_l, \mathbf{q}_r$. For the Euler equations of gas dynamics a Roe mean value is given by

$$\begin{aligned} \tilde{\rho} &= \sqrt{\rho_l \rho_r}, \\ \tilde{u} &= \frac{\sqrt{\rho_l} u_l + \sqrt{\rho_r} u_r}{\sqrt{\rho_l} + \sqrt{\rho_r}}, \\ \tilde{v} &= \frac{\sqrt{\rho_l} v_l + \sqrt{\rho_r} v_r}{\sqrt{\rho_l} + \sqrt{\rho_r}}, \\ \tilde{w} &= \frac{\sqrt{\rho_l} w_l + \sqrt{\rho_r} w_r}{\sqrt{\rho_l} + \sqrt{\rho_r}}, \\ \tilde{H} &= \frac{\sqrt{\rho_l} H_l + \sqrt{\rho_r} H_r}{\sqrt{\rho_l} + \sqrt{\rho_r}}, \\ \tilde{c} &= \sqrt{(\gamma - 1) \left(\tilde{H} - \frac{1}{2} \tilde{v}^2 \right)} \end{aligned} \quad (7)$$

with $\tilde{v}^2 = \tilde{u}^2 + \tilde{v}^2 + \tilde{w}^2$ in the full three-dimensional case. For 2d, we just have to omit the values for the third velocity component w . Similarly, we find a Roe mean value for the shallow water equations by

$$\begin{aligned} \tilde{h} &= \frac{1}{2} (h_l + h_r), \\ \tilde{u} &= \frac{\sqrt{h_l} u_l + \sqrt{h_r} u_r}{\sqrt{h_l} + \sqrt{h_r}}, \\ \tilde{v} &= \frac{\sqrt{h_l} v_l + \sqrt{h_r} v_r}{\sqrt{h_l} + \sqrt{h_r}}. \end{aligned} \quad (8)$$

Together with wave-wise application of standard upwind, this results in the numerical flux function

$$\mathbf{g}_{\text{Roe}}(\mathbf{q}_r, \mathbf{q}_l) = \frac{1}{2}(\mathbf{f}(\mathbf{q}_l) + \mathbf{f}(\mathbf{q}_r)) - \frac{1}{2} |\mathbf{A}(\tilde{\mathbf{q}})| \Delta \mathbf{q}, \quad (9)$$

where the absolute value is applied to the eigenvalues of the matrix. This numerical flux is usually referred to as the standard Roe solver and is an example for a complete flux. Note that the wave-wise application of schemes other than standard upwind would only affect the eigenvalues of the viscosity matrix. In this study, we do not use the solver in the form (9) but with the so called Harten-Hyman fix [20], which slightly increases the numerical viscosity at sonic rarefaction waves and thus prohibits the sonic glitch. The sonic glitch would otherwise lead to a representation of sonic rarefaction waves as rarefaction shocks. It is also possible to resemble the following HLL-type schemes by simply modifying the eigenvalues of the viscosity matrix in (9).

3.2.2 HLL

As an example of an incomplete flux, we employ HLL. In [21], Harten, Lax, and van Leer present and discuss a variety of numerical flux functions, the simplest and most robust of which is usually called HLL, a scheme with very low computational cost². Their basic idea is to start from conservation. First, one estimates $S_L \leq 0 \leq S_R$ for the bounding speeds of the Riemann problem given by left and right states $\mathbf{q}_l, \mathbf{q}_r$. If one uses conservation for rectangle $[S_l, S_r] \times [0, 1]$ in space and time, the mean value of the conserved quantities \mathbf{q} in the intermediate states of the Riemann problem can be computed. From this, by integration over $[S_l, 0] \times [0, 1]$ and $[0, S_r] \times [0, 1]$ and averaging, one obtains the numerical flux

$$\mathbf{g}_{\text{HLL}}(\mathbf{q}_r, \mathbf{q}_l) = \frac{1}{2}(\mathbf{f}(\mathbf{q}_r) + \mathbf{f}(\mathbf{q}_l)) - \frac{1}{2} \frac{S_R + S_L}{S_R - S_L} (\mathbf{f}(\mathbf{q}_r) - \mathbf{f}(\mathbf{q}_l)) + \frac{S_R S_L}{S_R - S_L} (\mathbf{q}_r - \mathbf{q}_l). \quad (10)$$

We assume now that $\tilde{\mathbf{A}} = \tilde{\mathbf{A}}(\mathbf{q}_l, \mathbf{q}_r)$ is a consistent local linearization, a so-called Roe matrix, and thus satisfies condition (3). Then (10) can be rewritten as

$$\mathbf{g}_{\text{HLL}}(\mathbf{q}_r, \mathbf{q}_l) = \frac{1}{2}(\mathbf{f}(\mathbf{q}_r) + \mathbf{f}(\mathbf{q}_l)) - \frac{1}{2} \frac{S_R + S_L}{S_R - S_L} \tilde{\mathbf{A}}(\mathbf{q}_r - \mathbf{q}_l) + \frac{S_R S_L}{S_R - S_L} (\mathbf{q}_r - \mathbf{q}_l). \quad (11)$$

Hence, the viscosity matrix of the HLL-flux is

$$\mathbf{V} = \frac{S_R + S_L}{S_R - S_L} \tilde{\mathbf{A}} - 2 \frac{S_R S_L}{S_R - S_L} \mathbf{I} \quad (12)$$

and has the same left and right eigenvectors as the Roe matrix $\tilde{\mathbf{A}}$ itself. The eigenvalues and thus the wave-wise viscosity coefficients are

$$\frac{S_R + S_L}{S_R - S_L} \tilde{\lambda}_k - 2 \frac{S_R S_L}{S_R - S_L} \quad (13)$$

²Their more elaborate solvers somehow anticipate HLLC [57]

with $\tilde{\lambda}_k$ being the eigenvalues of $\tilde{\mathbf{A}}$. Apparently, the choice of the bounding wave speeds is crucial for the numerical viscosity. In the literature, many choices of the wave speeds S_L, S_R are given. For an overview, the reader is referred to [58]. Here, we mainly rely on the choice suggested by Einfeldt [13]: If it is affordable to compute the leftmost and the rightmost wave speed of a consistent local linearization $\tilde{\lambda}_1$ and $\tilde{\lambda}_m$, and the flux function f is convex, then set

$$S_L = \min\{\tilde{\lambda}_1, \lambda_1(\mathbf{q}_l), 0\}, \quad S_R = \max\{\tilde{\lambda}_m, \lambda_m(\mathbf{q}_r), 0\}. \quad (14)$$

This ensures that for both a single discontinuity and a single rarefaction wave the estimate of the maximal and minimal wave speed is sharp. The resulting numerical flux is called *HLL*. Like the standard Roe scheme, it tries to force the Rankine-Hugoniot condition at shocks.

3.2.3 HLLEM

The first scheme that exploited the relation between Roe and HLL type schemes is the HLLEM scheme for gas dynamics by Einfeldt [13]. It is an attempt to formulate the Roe scheme as correction to HLL. There are several advantages: The computational effort is reduced, the adjustment of the viscosity on the acoustic waves can be easily applied by choosing the bounding speeds S_L and S_R , the sonic point glitch can be avoided, and the failure of the standard Roe scheme for strong rarefaction waves can be healed.

The construction is as follows: For the sake of simplicity, we assume for the eigenvalues $\tilde{\lambda}_1 \leq \tilde{\lambda}_2 \leq \dots \leq \tilde{\lambda}_m$ of the Roe matrix $\tilde{\mathbf{A}}$ that $\tilde{\lambda}_1 \leq 0 \leq \tilde{\lambda}_m$. Thus, we can choose $S_L = \tilde{\lambda}_1$ and $S_R = \tilde{\lambda}_m$. With this setting, the viscosity matrix of the Roe scheme can be written as

$$\mathbf{V}_{\text{Roe}} = \mathbf{V}_{\text{HLL}} + \frac{S_R S_L}{S_R - S_L} \tilde{\mathbf{R}} \mathbf{K} \tilde{\mathbf{L}} \quad (15)$$

$$= \mathbf{V}_{\text{HLL}} + \frac{\tilde{\lambda}_m \tilde{\lambda}_1}{\tilde{\lambda}_m - \tilde{\lambda}_1} \tilde{\mathbf{R}} \mathbf{K} \tilde{\mathbf{L}} \quad (16)$$

with the anti-diffusion-matrix

$$\mathbf{K} = \text{diag}(0, \delta_2, \dots, \delta_{m-1}, 0). \quad (17)$$

For the two-dimensional Euler equations ($m = 4$), we find for the so-called anti-diffusion-coefficients

$$\delta_2 = \delta_3 = 2 \left(1 - \frac{|\tilde{u}|}{\tilde{c} + |\tilde{u}|} \right). \quad (18)$$

The special structure K allows us to express the standard Roe flux by only using the eigenvectors corresponding to the entropy and shear wave. Park and Kwon [46] show that, independent of the choice of S_L and S_R , HLLEM resolves single contact waves exactly when adhering to the Roe mean values for the anti-diffusion-term, i. e. if we stick to (16) instead of (15) as originally suggested by Einfeldt. For HLLEMCC, our modification of

HLLM as discussed in the next section, we nevertheless employ the original Einfeldt setting (15). The loss in resolution of the scheme is rather small. An advantage of (15) is that it deactivates the anti-diffusion terms automatically for full upwind, i. e. if one of the bounding speeds S_L, S_R vanishes.

A special case of HLLM is obtained if we set $S_R = -S_L = |S_{\max}|$. In gas dynamics and shallow water flow, the numerical viscosity of the resulting scheme coincides with the viscosity of the Rusanov/LLF (Local Lax Friedrichs) scheme for nonlinear waves and with the viscosity of the standard Roe scheme for shear and entropy waves. In the following, we refer to that scheme as LLFEM.

3.2.4 HLLMCC

If in the definition of the HLLM scheme, we replace the anti-diffusion coefficients δ_k by $(1 - \phi)\delta_k$ with $\phi \in [0, 1]$, we can smoothly vary between HLLM ($\phi = 0$) and HLL ($\phi = 1$), i. e. between a complete and an incomplete Riemann solver. This is a technique which we used for our carbuncle cure of HLLM (HLLMCC) in [25] for the Euler equations and in [29] for the shallow water equations.

Since the goal of HLLMCC is to prevent unphysical shear and entropy waves, its core is the computation of the residual in the Rankine-Hugoniot condition for these waves:

$$\tau = f(q_r) - f(q_l) - \tilde{u}(q_r - q_l) \quad (19)$$

with the Roe mean value for the normal velocity \tilde{u} . Now, we take as our basic indicator the residual relative to \tilde{c} , respectively its Euclidean norm

$$\theta = \frac{1}{\tilde{c}} \|\tau\|_2, \quad (20)$$

which vanishes for all shear and entropy waves. By introducing parameters $\alpha, \beta \in (0, 1)$, we can now define

$$\phi(\theta, Fr_u) = \min\{1, \varepsilon \theta \max\{0, (1 - Fr_u^\alpha)\}\}^\beta \quad (21)$$

for shallow water and

$$\phi(\theta, M_u) = \min\{1, (\varepsilon \theta)^\beta \max\{0, (1 - M_u^\alpha)\}\} \quad (22)$$

for the Euler equations, where Fr_u and M_u are the directional Froude and Mach numbers perpendicular to the cell face. A major advantage of this approach is that the modification can be applied to shear and entropy waves separately. This we will use in Section 6.2 to somehow measure the influence of both wave types on the carbuncle.

However, we still have to choose the parameters. Here, we adhere to the values as already published [3, 25, 28, 29]: For both shallow water and gas dynamics $\alpha = \beta = .33$ turned out to be a good choice. Furthermore, if not stated otherwise, we use $\varepsilon = 1/100$ in the gas dynamics case and for the shallow water equations $\varepsilon = 10^{-3}$.

3.2.5 Shock fix

While HLEMCC modifies the numerical viscosity of HLEM on the linearly degenerate waves, here we present a modification of the numerical viscosity at shocks. We will restrict to steady shocks in the Euler equations. Again we employ the residual in the Rankine-Hugoniot condition but this time on the nonlinear waves:

$$\tau = \mathbf{f}(\mathbf{q}_r) - \mathbf{f}(\mathbf{q}_l) - (\tilde{u} - \tilde{c})(\mathbf{q}_r - \mathbf{q}_l) = \tilde{c} (\mathcal{W}_2 + \mathcal{W}_3 + 2\mathcal{W}_2), \quad (23)$$

for shocks in the left wave, and for shocks in the right wave

$$\tau = \mathbf{f}(\mathbf{q}_r) - \mathbf{f}(\mathbf{q}_l) - (\tilde{u} - \tilde{c})(\mathbf{q}_r - \mathbf{q}_l) = -\tilde{c} (2\mathcal{W}_1 + \mathcal{W}_2 + \mathcal{W}_3). \quad (24)$$

Instead of using the residual in the Rankine-Hugoniot condition relative to the speed of sound, we employ the sum of the fluxes as our weighting factor. If we take the shock indicator

$$\theta_s = \varepsilon_s \left(1 - \frac{\|\mathbf{f}(\mathbf{q}_r) - \mathbf{f}(\mathbf{q}_l)\|_2}{\|\mathbf{f}(\mathbf{q}_r) + \mathbf{f}(\mathbf{q}_l)\|_2} \right) \quad (25)$$

with some small positive parameter ε_s , we can modify the Einfeldt choice of wave speeds (14) to

$$\begin{aligned} S_L &= \min\{\theta_s(u_l - c_l) + (1 - \theta_s)(\tilde{u} - \tilde{c}), u_l - c_l, 0\}, \\ S_R &= \max\{\theta_s(u_r + c_r) + (1 - \theta_s)(\tilde{u} - \tilde{c}), u_r + c_r, 0\} \end{aligned} \quad (26)$$

resulting in a HLEM-solver that does not enforce the Rankine-Hugoniot condition at steady shocks. In fact, the numerical viscosity is slightly increased as like in the Osher scheme, which we describe next.

3.3 Osher-Solomon

The Osher-Solomon scheme [44], a generalization of the Enquist-Osher scheme [15] to systems of conservation laws, was designed with two major goals: prevent the sonic glitch and represent physically steady states as discrete steady states. For that purpose, they first had to abandon the Rankine-Hugoniot condition at shocks as a design principle. Instead, they use (generalized) Riemann-invariants. While this would lead to a slightly increased numerical viscosity at shocks, it also allows for stable steady state representations of steady shocks. Thus, the scheme is a good candidate for our purposes: measure the influence of the stability of the shock position on the carbuncle. The resulting numerical flux function reads as

$$\mathbf{g}_{\text{Osher}}(\mathbf{q}_l, \mathbf{q}_r) = \frac{1}{2} (\mathbf{f}(\mathbf{q}_r) + \mathbf{f}(\mathbf{q}_l)) - \frac{1}{2} \int_{\Gamma} |\mathbf{A}(\mathbf{q})| d\mathbf{q}, \quad (27)$$

where Γ is a path in the state space which connects the left and right state via integral curves. Later on, Hemker and Spekreijse [22] presented an alternative choice for Γ , which they claim leads to better results. But, since in our tests we could not find any difference between the results of both versions, we just refer to it as Osher-scheme without differentiating for the integration path in (27).

4 Discussion of the test cases for the numerical investigation of the carbuncle

In our discussion of the carbuncle and its sources, the choice of test cases plays an important role. They include classical examples like the double Mach reflection and the blunt body problem, which gave rise to the name of the carbuncle [47], as well as some $1\frac{1}{2}$ -dimensional problems like the colliding flow problem, the steady shock, and the Quirk test. These tests have in common that they originate from one-dimensional problems which are artificially augmented with an additional space dimension. Since in these physically one-dimensional problems there is no inherent source for the carbuncle, we have to trigger it by adding some noise to the initial data. While most of these test cases have in common that in a physical sense we would not expect to see a carbuncle, the opposite is observed for the Elling test as drawn from the considerations in Section 2.3.

4.1 Blunt body problem

In gas dynamics, a popular test case for the carbuncle is the flow around a cylindrical obstacle [9, 12, 31, 45, 46, 48, 53]. In the shallow water case, a similar test would be the flow around a cylindrical bridge pier. We chose a pier with radius $r = 1$. As computational domain we employ a third of the annulus with inner radius $r = 1$ and outer radius $R = 2$. Since the interesting part of the flow is the inflow region, we restrict the domain in angular direction to $\frac{2\pi}{3}, \frac{4\pi}{3}$. The domain is discretized with 150 cells in the radial direction and 800 cells in the angular direction. The initial flow is set to the inflow state everywhere. At the pier we employ wall boundary conditions, at the other boundaries first order extrapolation.

Although, in principle, it is possible to do comparisons for blunt body flow also in the gas dynamics case [28], here we restrict our investigation to shallow water. Since we want to start with the initial flow set to the inflow state, we could employ the gas dynamics version of the Osher scheme only for subsonic inflow. Thus, in this paper, we only show results for the shallow water case. For the inflow we choose Froude number $Fr = 5$.

4.2 Double Mach reflection

A famous test for the quality of a Riemann solver is the Double Mach reflection problem. It was suggested by Woodward and Colella [62] as a benchmark for Euler codes. An analytical treatment is found in [39], [5], and references therein, while experimental results are presented in [19] and also in [5, pp. 152 and 168]. The problem consists of a shock front that hits a ramp which is inclined by 30 degrees. When the shock runs up the ramp, a self-similar shock structure with two triple points evolves. The situation is sketched out in Figure 2. To simplify the graphical representation, the coordinate system is aligned with the ramp – as done for the numerical tests. In the primary triple point, the incident shock i , the mach stem m , and the reflected shock r meet. In the double Mach configuration, the

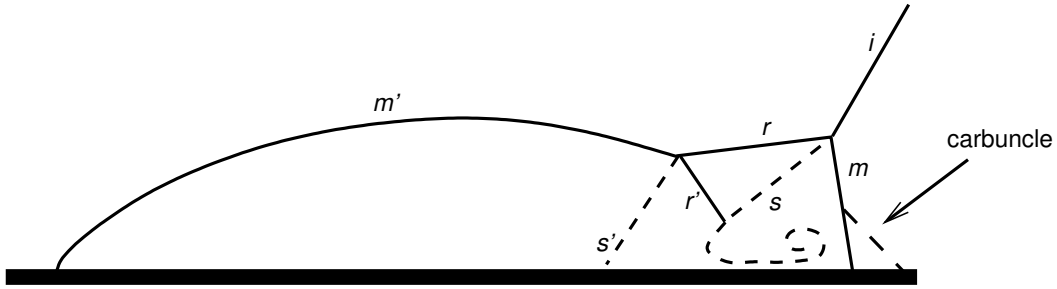


Figure 2: Sketch of Double Mach Reflection with the carbuncle-type numerical artifact resulting in a kink in the leading Mach stem m .

reflected shock breaks up forming a secondary triple point with the reflected shock r , a secondary (bowed) Mach stem m' , and a secondary reflected shock r' . From both triple points, slip lines emanate. The reflected shock r' hits the primary slip line s causing a curled flow structure.

While the main challenge for a high resolution scheme is to resolve the secondary slip line s' [30, 62], the main challenge for first and second order schemes is to correctly represent the leading Mach stem. For some lower order schemes, the lower end of the Mach stem moves too fast, leading to a kink in the stem [48]. The situation is comparable to that for the blunt body problem. According to the wall boundary conditions, the ramp can be interpreted as the symmetry-line of a free-stream flow. Since the Mach stem is not perfectly aligned to the grid lines of a Cartesian grid, the same mechanisms come into place as for the blunt body problem. Thus, we expect Riemann solvers which produce a carbuncle for the blunt body to behave similar in that case. If the flow is split at the symmetry-line by reinterpreting it again as a wall (or ramp), we have to expect the lower part of the Mach stem to be kinked as sketched out in Figure 2.

For the numerical tests in this paper, we follow the guidelines in [30]. That means the boundary conditions at the upper boundary model a slightly smeared shock, and the vertical size of the computational domain is doubled compared to [62]. The only difference is that, instead of the vertical momentum, we choose the entropy for our plots.

4.3 Colliding flow

This test [38, Section 7.7] resembles a simplified model for the starting process of the blunt body test when using the inflow state as initial data in the complete computational domain. This is best understood when considering the flow before the blunt body along the symmetry line. Since the flow is aligned with that symmetry line, and due to the switch of the sign of the flow velocity in wall boundary conditions, it behaves essentially like the left half of a colliding flow in 1d. To turn it into a 2d-test, the flow is equipped with an additional space direction, in which everything is expected to be constant. In order to trigger the carbuncle, the initial state is superimposed with noise that is generated randomly

and has a small amplitude.

For the gas dynamics test, in the initial state, density and pressure are set to $\rho = 1$, $p = 1$. The normal velocity is set to $u_{\text{left/right}} = \pm 20$, the transverse velocity component to $v = 0$. To trigger the carbuncle, we superimpose artificial numerical noise of amplitude 10^{-6} onto the primitive variables instead of disturbing it in just one point as was done originally by LeVeque [38, Section 7.7]. The computations are done on $[0, 60] \times [0, 30]$ discretized with 60×30 grid cells.

For shallow water tests, we set the initial height to $h = 1$ and the left and right velocities to $u = \pm 30$. The transverse velocity is zero. Onto this initial state, we superimpose artificial numerical noise of amplitude 10^{-6} , but in this case we add the noise to the conserved variables. The computations are done on $[-2.5, 2.5] \times [-2.5, 2.5]$ discretized with 40×40 grid cells.

Since the problem is a simple 2d-extension of a one-dimensional problem, the results are presented in scatter-type plots: we slice the grid in x -direction along the cell faces and plot the entropy for all slices at once.

4.4 Steady shock

While the colliding flow test models the starting process of the blunt body flow, the steady shock test, introduced by Dumbser et al. [12], features a simplified model for the converged shock in the blunt body flow. Following Dumbser et al., we set in the upstream region $\rho = 1$, $u = 1$. The upstream Mach number is set to $M = 20$, the transverse velocity component to $v = 0$. The shock is located directly on a cell face. To trigger the instability of the discrete shock profile, we add artificial numerical noise of amplitude 10^{-6} to the primitive variables in the initial state. The computations are done on $[0, 100] \times [0, 40]$ discretized with 100×40 grid cells.

For shallow water we set the water height and the Froude number at the inflow to $h = 1$ and $Fr = 30$ respectively. At the outflow, we simply employ extrapolation boundary conditions. Again, we add artificial numerical noise, this time of amplitude 10^{-3} , to the conserved variables in the initial state. The computations are done on $[-2.5, 2.5] \times [-2.5, 2.5]$ discretized with 100×40 grid cells.

Again for the presentation of the results, we employ scatter-type plots as described for the colliding flow problem.

4.5 Quirk test

Quirk [48] introduced a test problem which is known as Quirk test. Contrary to the preceding example, it is not a one-dimensional Riemann problem, but consists of a shock running down a duct. The shock is caused by Dirichlet-type boundary conditions on the left boundary with $\rho = 5.26829268$, $u = 4.86111111$, $p = 29.88095238$, while the flow field is initialized with $\rho = 1$, $u = v = 0$, $p = 1/\gamma$. Originally, a disturbance of the middle grid line was used to trigger the instability [48]. Because the computations are done with

a Cartesian code, we instead use numerical noise in the same manner as for the steady shock and the colliding flow problem. The only difference lies in the amplitude of the perturbation, here 10^{-3} . The computations are done on $[0, 1600] \times [0, 20]$ discretized with 1600×20 grid cells. In this study, we only perform the test for the Euler equations. For a similar test in shallow water, we refer to [3].

Again we use scatter-type plots (as described above) to present the results.

4.6 Elling test

The Elling test is the experiment which was already described in Section 2.3. The initial condition is a modified version of the steady shock test, cf. Section 4.4. The region to the right of the shock remains unchanged. In the supersonic inflow region, only the middle x -slice is changed. Here the velocity is set to zero. This is done to model a vortex layer hitting the shock front. Again, we only perform the test for the Euler equations and refer to [3] for a similar test in shallow water.

5 Influence of one-dimensional issues

Although the carbuncle is a multi-dimensional issue, it is obvious that, especially on Cartesian grids, one-dimensional issues can drive multi-dimensional effects.

5.1 Instability of shock position in first order schemes

Two of the instabilities discussed in Section 2 are purely one-dimensional. Both are instabilities of the shock: the instability of the shock position relative to the grid (Sec. 2.1) and the instability and ambiguity of the shock position within the grid cell (Sec. 2.2). Figure 3 illustrates how the instability of the shock position can destroy a discrete shock profile. As Bultelle et al. [7] point out, the shock position might jump by up to two grid cells. Figure 3 shows the worst case scenario: in one grid slice, it jumps two cells upstream, in the neighboring slice, it jumps two cells downstream. Thus, at a length of four grid faces, we created a new Riemann problem with all types of waves [28]. In the depicted situation, a strong flow downwards would be initiated. The instabilities and the ambiguity discussed in Section 2.2 can affect the discrete shock profile in a similar way. Since they are highly sensitive for perturbations, cross-flow might be induced within the grid slice containing the original shock itself.

This situation could be avoided if the 1d shock position was stable. However, as seen from the discussions in Sections 2.1 and 2.2, this would mean to abandon the requirement of Riemann solver which exactly reproduces the Rankine-Hugoniot condition at a single shock. As mentioned above, the Osher solver replaces this by the requirement of yielding steady discrete solutions for any steady discontinuity and employs Riemann invariants over all nonlinear waves. Thus, the Osher scheme seems to be a good candidate to avoid

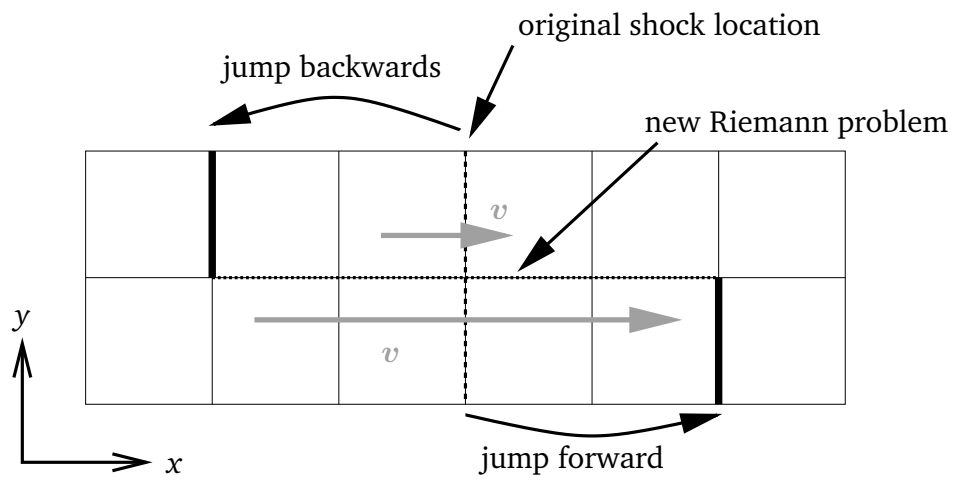


Figure 3: Unstable two-dimensional shock profile

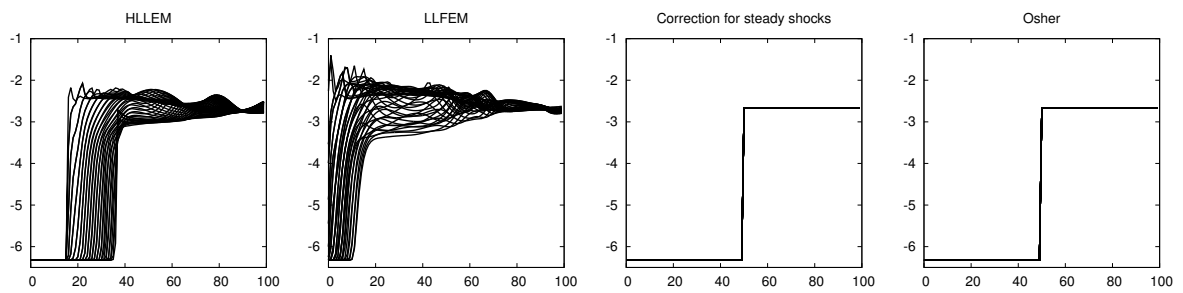


Figure 4: Scatter-type plots of entropy for steady shock with different numerical fluxes at $t = 1000$.

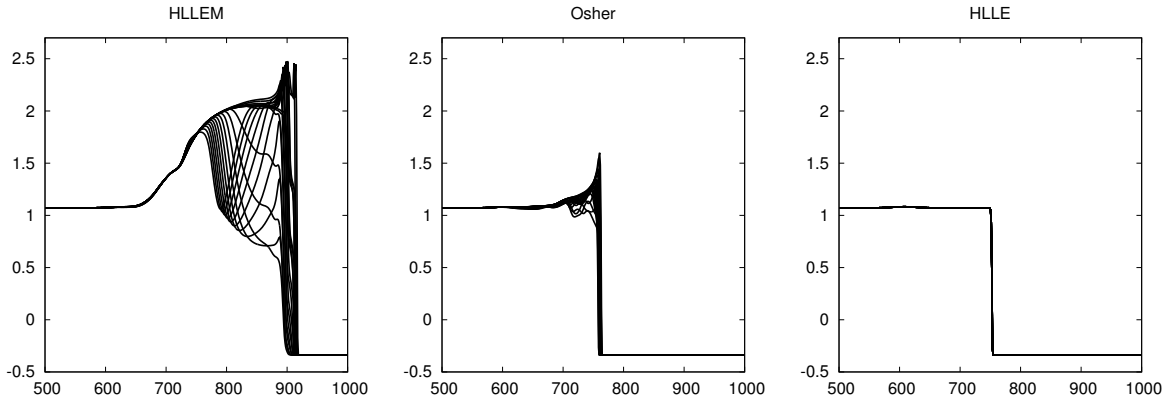


Figure 5: Scatter-type plots of entropy for Quirk test with different numerical fluxes at $t = 125$.

the instability of the 1d shock position, much the same as the HLLM-scheme with the modification at steady shocks (Sec. 3.2.5). Another solver which also disregards the Rankine-Hugoniot condition is LLFEM. The difference to Osher and the steady shock fix is that the numerical viscosity on the nonlinear waves is much higher. As the results in Figure 4 show, the LLFEM cannot prevent the carbuncle while the other two can. From that, we conclude that it is important to add the correct amount of viscosity in order to stabilize the shock position.

Figure 5 reveals that if we guarantee steady discrete representations of steady states this is not sufficient to guarantee a proper representation of unsteady flows. The Quirk test is employed and shows that the Osher scheme still might produce carbuncle-like structures, although much weaker than with, e. g., HLLM.

Our setting for the blunt body problem results in a highly transient starting phase which eventually passes into a steady state. This raises the question which property of the Osher scheme would be dominant: the tendency to produce a carbuncle in a transient flow or the guarantee for steady discrete representations of steady flows. Thus, in Figure 6, we show the shallow water flow around a cylindrical pier at different times. At time $t = 1.5$, it is easy to see that the scheme produces a slight carbuncle-type structure. When the discrete flow field eventually becomes steady, obviously that carbuncle is somehow smoothed out. The solution is steady but not physical, confirming the statement by Robinet et al. [49] that the carbuncle can lead to unphysical steady states.

5.2 Influence of the order of the scheme

Since it is often reported that increasing the order of the scheme applied in the computation reduces the carbuncle, here we investigate the relation between the order of the scheme and the 1d-stability of the discretized shock. At this point, we should stress out that throughout this paper the term *order* refers to the design order of the scheme, which is only achieved

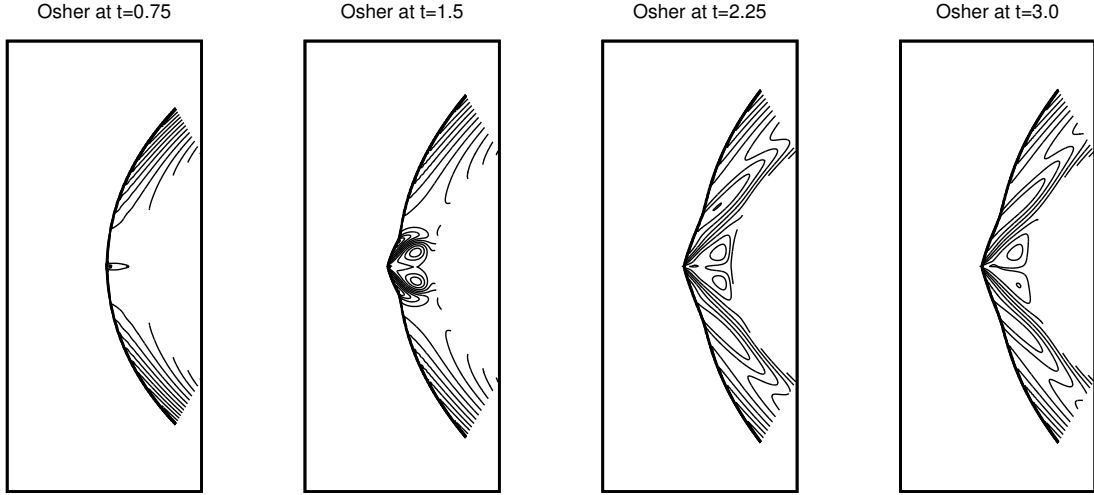


Figure 6: Flow around cylindrical pier in shallow water with 1st order Osher scheme at different times. Energy shown.

in smooth parts of the flow field, and not to the actual order of the scheme which would automatically drop in the vicinity of shocks. As was pointed out by Roe and Zaide [63–65], a major role is played by the fact that it is impossible, at least for gas dynamics and shallow water flows, to split a shock satisfying the Rankine-Hugoniot condition into two consecutive shocks which both would satisfy the Rankine-Hugoniot condition. This situation improves for higher order, at least when geometric reconstruction is applied. For the computation of the inter-cell fluxes, two states are available, one at the left cell boundary and one at the right cell boundary. Thus, for a steady shock it would be sufficient to satisfy

$$f(q_l) = f(q_m^-) = f(q_m^+) = f(q_r), \quad (28)$$

which can easily be achieved by

$$q_m^- = q_l, \quad q_m^+ = q_r. \quad (29)$$

This is (for a scalar situation) sketched out in Figure 7. For the sake of simplicity, in the following, we restrict our considerations to the scalar case. It is easy to see how the results can be transferred back to the systems case.

Figure 7 shows how the situation improves with increasing order of the scheme. If, for instance, we employ a polynomial reconstruction in the cell where the shock is located, for high orders, condition (29) can be ensured for almost all shock positions without sacrificing monotonicity:

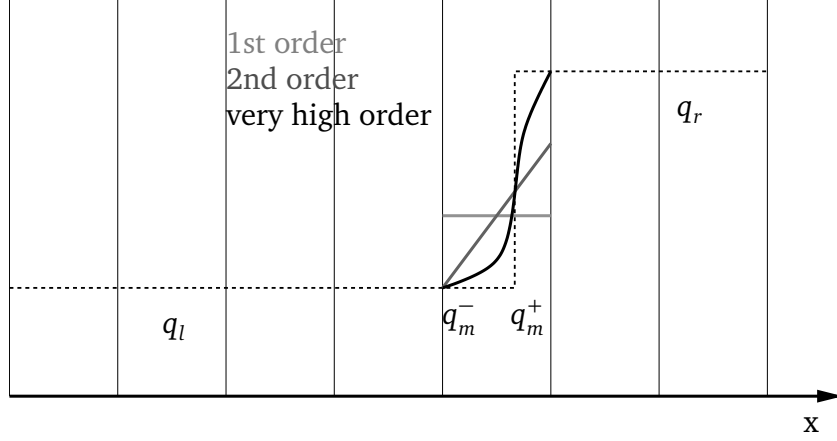


Figure 7: Reconstruction of shock profile (dashed line) on finite volume grid with different orders

Theorem 1. *Given the situation depicted in Figure 7, let the cell with the shock be $[x_{i-1/2}, x_{i+1/2}]$ and $\Delta x = x_{i+1/2} - x_{i-1/2}$. Furthermore let $\Delta q = q_r - q_l \neq 0$. Let the shock be located at $x_{i-1/2} + \theta \Delta x$ with $\theta \in [0, 1]$.*

1. *For any $\theta \in [0, 1]$, a polynomial reconstruction $p_{(n)}$ with degree less or equal two can be found such that condition (29) is satisfied.*
2. *In the cell $[x_{i-1/2}, x_{i+1/2}]$, the reconstruction can be made monotone for polynomial degree $\leq n$ if $\theta \in [\frac{1}{n+1}, 1 - \frac{1}{n+1}]$.*

Proof. Statement 1 is obvious and well known. It was already used by van Leer in his work on higher order methods [60].

For the proof of statement 2, we can assume, without restriction,

$$[x_{i-1/2}, x_{i+1/2}] = [0, 1], \quad q_l = 0, \quad q_r = 1, \quad \text{and} \quad \theta \geq 1/2.$$

All other cases can be derived from this by symmetry, scaling, and translation.

It is easy to see that with above settings

$$\int_0^1 q(x) dx = 1 - \theta. \quad (30)$$

On the other hand, we know for any monomial

$$\int_0^1 x^n dx = \frac{1}{n+1}. \quad (31)$$

Furthermore all monomials with degree greater of equal one are monotonously increasing in $[0, 1]$ and attain the values 0 at $x = 0$ and 1 at $x = 1$. Obviously, the same is true for

all weighted means of such polynomials as long as the weights are non-negative. Thus, for any $\theta \in [\frac{1}{2}, \frac{1}{n+1}]$, we can find a polynomial p_n of degree $\leq n$, monotonously increasing in $[0, 1]$, with

$$p_n(0) = 0, \quad p_n(1) = 1, \quad \text{and} \quad \int_0^1 p_n(x) dx = 1 - \theta. \quad (32)$$

As already mentioned, the general case follows from this by symmetry, scaling, and translation. \square

Note that the linear reconstruction of case 1 in Theorem 1 is not achieved by standard second order schemes. Due to their restricted stencil, they cannot distinguish between the situation of Theorem 1, case 1 (slope $\Delta q/\Delta x$ in the middle cell), and a linear state with slope $\Delta q/(2\Delta x)$. But in order to achieve second order, they have to reconstruct linear states exactly. Slope $\Delta q/\Delta x$ in the middle cell can be achieved, e. g., by the limiter φ_{Sweby} , the upper bound of the Sweby region, as described in [26, Section 2.4.2], leading to a first order scheme. For other $\theta \in [-1, 1]$ it would still satisfy one of the identities (29). While Minmod cannot satisfy any of the identities (29) for $\theta \in (-1, 1)$, Superbee shares the behavior of φ_{Sweby} for $|\theta| \geq 1/3$ and the MC-Limiter for $|\theta| \geq 1/2$.

In this context, it is also worth to note that some third order schemes, although formally based on linear reconstructions, e. g. [2, 8] in the final analysis still employ parabolic reconstructions. For each cell, they compute two linear reconstructions in the manner described in [26, Section 2.4.2], one ensuring third order for left-going waves and another one ensuring third order for right-going waves. While q_m^- is taken from the first reconstruction, q_m^+ is taken from the latter. Although it is, in general, not possible to reinterpret this as a single linear reconstruction, it is always possible to reinterpret it as a parabolic reconstruction. But due to their restricted stencil, they do, in general, not satisfy the identities in equation (29). Strangely enough, none of the authors of such limiters considers the resulting parabolic reconstruction, and, therefore, none of them checks if this parabolic reconstruction is indeed monotone.

Since many modern schemes, like ENO/WENO, do not explicitly enforce monotone reconstructions in the cells, for these schemes, we can expect identities (29) to be satisfied in most cases, and, if not so, at least approximated with very small error. Thus, for schemes of order greater or equal three, we might expect physically steady shocks to be represented as discrete steady shock, independent of the Riemann solver and the position of the shock, and hope for a similar behavior for moving shocks.

6 Influence of two- or three-dimensional issues

For years, the research on the carbuncle concentrated on two-dimensional issues, although the Osher scheme was already in widespread use, and the carbuncle was known to be rarely found in very high order schemes or on unstructured grids. Here, we started with

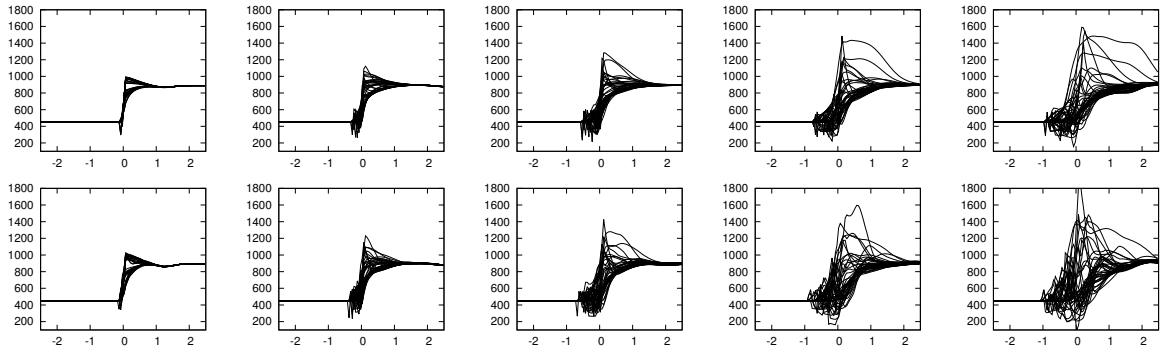


Figure 8: Steady shock problem in shallow water at times $t = 0.2, 0.4, 0.6, 0.8, 1.0$ with Roe scheme, energy shown. Upper row: first order; second row: second order with Superpower limiter.

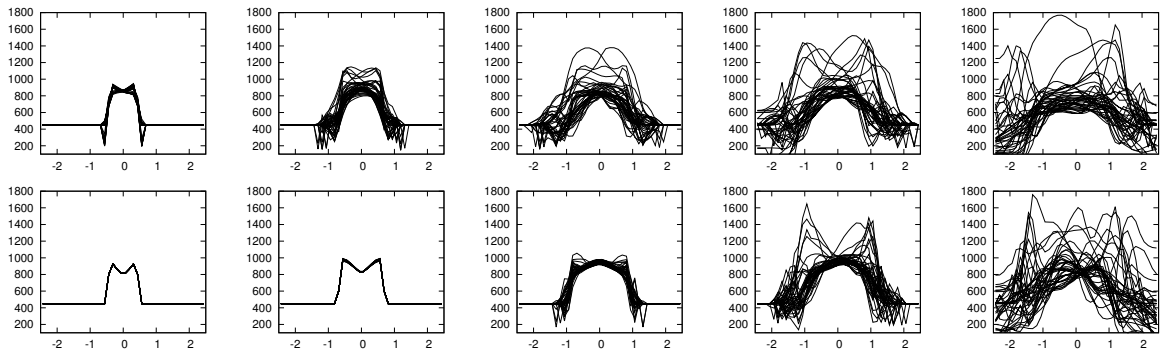


Figure 9: Colliding flow problem in shallow water at times $t = 2/3, 1, 4/3, 5/3, 2$ with Roe scheme, energy shown. Upper row: first order; second row: second order with Superpower limiter.

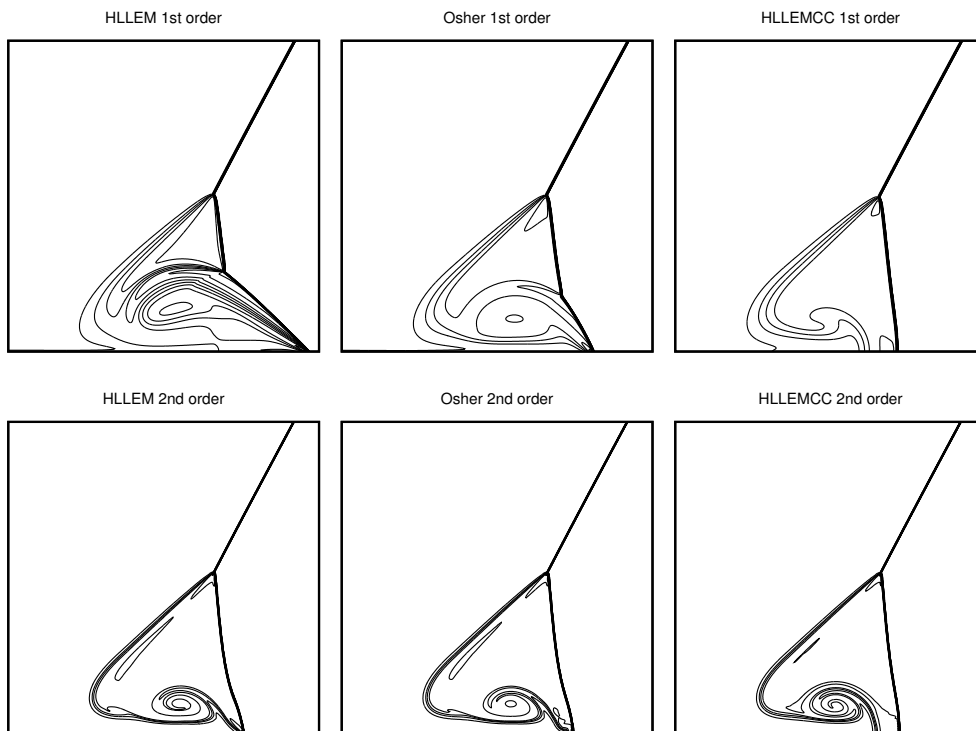


Figure 10: Leading shock structure of double Mach reflection in gas dynamics at $t = 0.2$ with different numerical fluxes, entropy shown. Upper row: first order, lower row: second order.

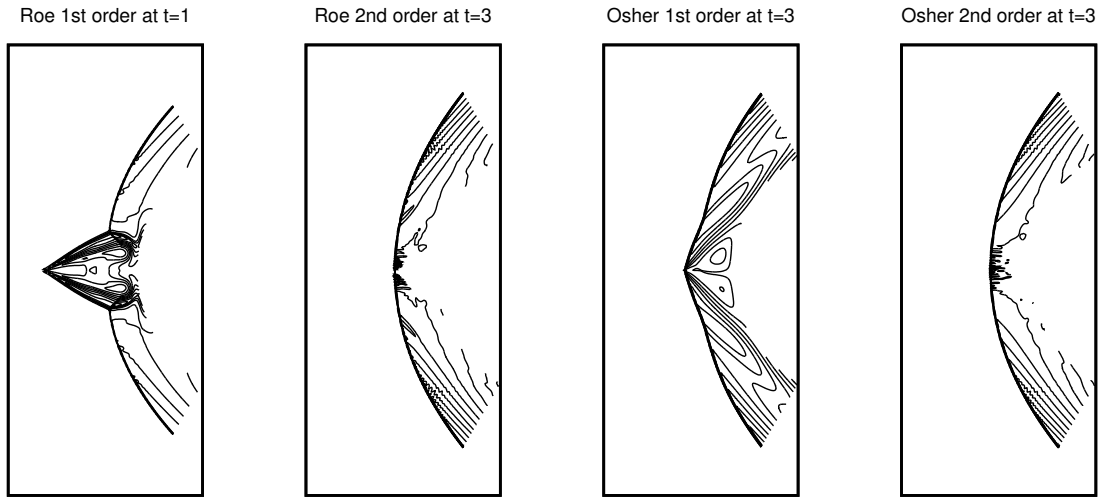


Figure 11: Flow around cylindrical pier in shallow water at Froude number $Fr = 5$ with Roe and Osher, first order and second order with Albada 3.

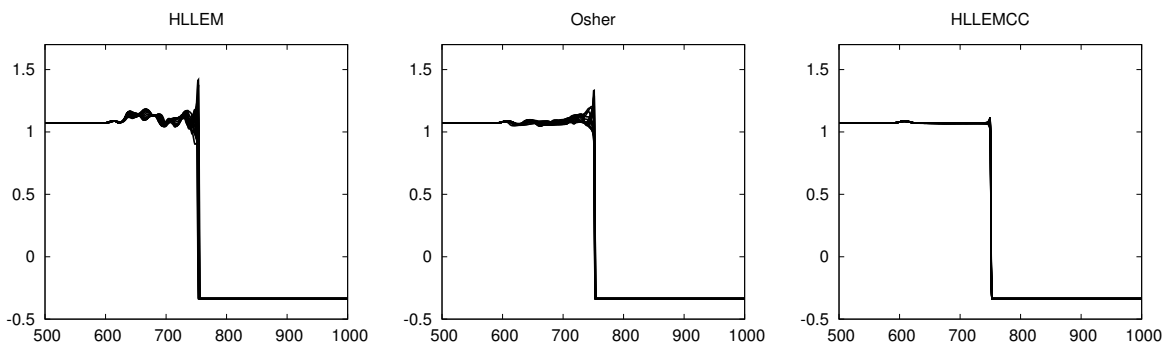


Figure 12: Scatter-type plots of entropy for Quirk test with different numerical fluxes and second order at $t = 125$.

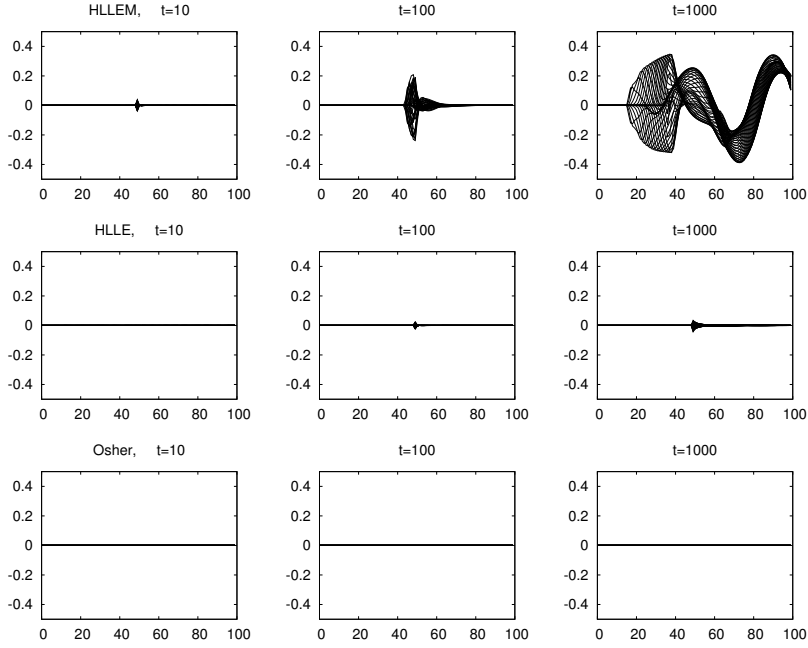


Figure 13: Transverse velocity at different times in gas dynamics steady shock problem for different solvers.

one-dimensional issues to better understand how they, when everything is generalized to two or three space-dimensions, interact with two- and three-dimensional issues. Hence, in this section, we want to concentrate on the interplay of 1d and 2d (or 3d) issues.

6.1 Numerical shear viscosity

At this point, we have to refer the reader back to Figure 3. It is obvious that the vertical flow induced by the instability of the shock position in turn induces a strong shear flow not only in the newly created Riemann problem, but even more along the original shock profile. In summary, some kind of turbulence at the original shock position is created which is superimposed onto the original flow. Due to its construction, the HLLMCC solver distinguishes between shear waves which are superimposed onto nonlinear waves and shear waves which are not. On the first, it behaves like HLL, thus damping the turbulence, on the latter, it behaves like HLLM, here allowing, e. g., for well resolved boundary layers. In our previous works [3, 25, 28, 29], we could show that HLLMCC prevents the carbuncle while allowing for good resolution of physical shear waves.

In Figure 13, we demonstrate how the above described mechanism drives the carbuncle. We show the transverse velocity at different times for HLLM, HLL, and the Osher scheme. By stabilizing the 1d shock position, the Osher scheme keeps the transverse velocity at about the magnitude of the artificial numerical noise introduced in the initial state. Thus, no carbuncle arises. The HLL scheme, by its excessive shear viscosity, keeps the transverse

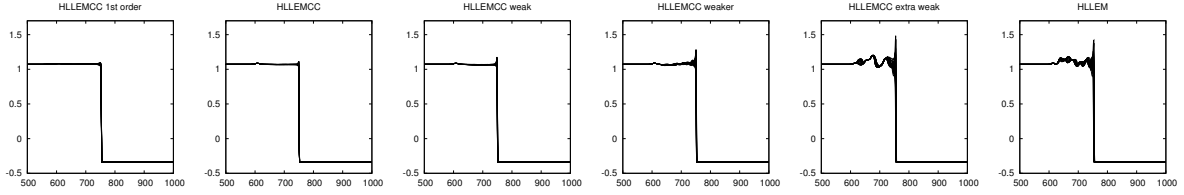


Figure 14: Quirk test at $t = 125$ with 1st order standard HLEMCC and different versions of 2nd order HLEMCC scheme.

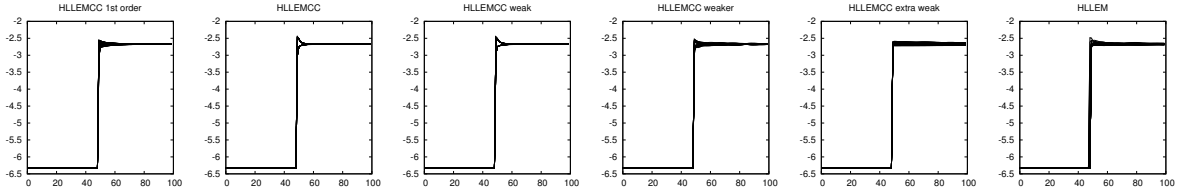


Figure 15: Steady shock in gas dynamics at $t = 1000$ with 1st order standard HLEMCC and different versions of 2nd order HLEMCC scheme.

velocity below some threshold and thus also avoids the carbuncle. For HLEM, there is no mechanism to damp the turbulence along the original shock. Over time, a carbuncle evolves.

6.1.1 Shear viscosity and order of the scheme

As we have seen in Section 5.2, higher order has a stabilizing effect on the 1d shock position. This raises the question if for second order schemes, the carbuncle correction in HLEMCC might be relaxed. The answer is not obvious since raising the order also lowers the viscosity on the shear waves. In Figure 14, we give a comparison of first order HLEMCC and several implementations with second order. The difference between the versions is in the choice of the parameters. As mentioned in Section 10, for the standard HLEMCC, the parameter ε in equations (21) and (22) is chosen as $\varepsilon = 0.01$. Here we also show results for $\varepsilon = 0.005$, $\varepsilon = 0.00125$, and for $\varepsilon = 10^{-6}$. For the latter, the results are almost indistinguishable from the pure second order HLEM. All in all, the results suggest to leave the parameters unchanged and stay with the same parameters as in the standard version for first order. The gain in stability of the 1d shock position and the loss in shear viscosity are just in balance. For the steady shock test in Figure 15, the situation slightly improves. But it is still recommended to use HLEMCC with the set of parameters given in Section 3.2.4.

6.1.2 Shear viscosity and the resolution of physical carbuncles

In Section 2.3 we discussed the findings of Elling [14] on physical carbuncles. This lead us to the Elling test case as described in Section 4.6 which allows us to test the numerical flux functions for their ability to resolve these physical carbuncles correctly. As we can see from

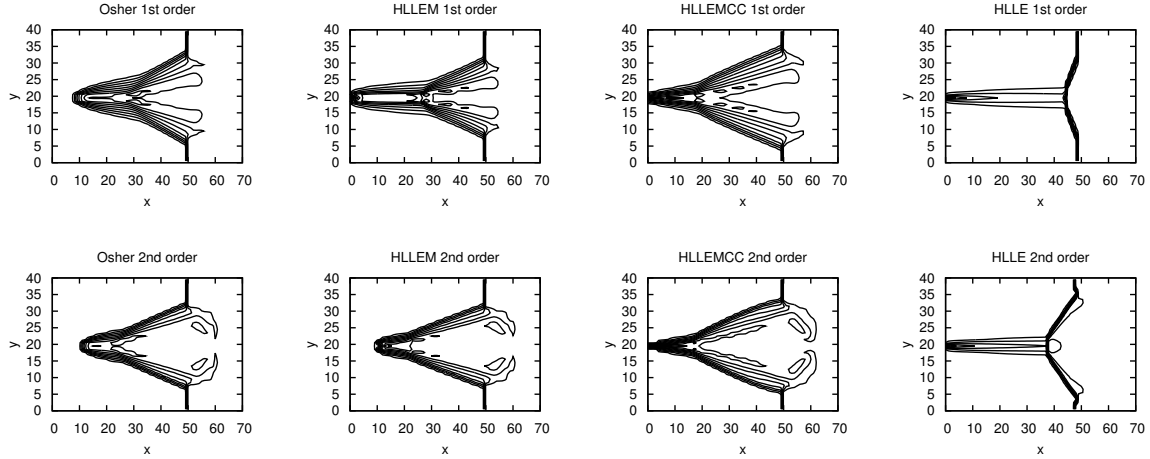


Figure 16: Elling test for gas dynamics at time $t = 100$; comparison of different solvers; entropy shown.

Figure 16, the numerical results with Osher, HLEM, and HLEMCC are rather similar even with the first order scheme. The HLE scheme, which suppresses the carbuncle by a severe amount of numerical shear viscosity, tries to prevent even the physical carbuncle, not only in the first order, but also in the second order computation. Since the test case is a model for shock boundary-layer and other shock vortex interactions, we note that schemes which rely on the HLE flux, even when it is only applied locally in the vicinity of strong shocks, might destroy some physical features of the flow. Thus, codes which are based on a switch between complete and incomplete Riemann solvers depending on the distance to the next strong shock should be carefully tested with the Elling test before applying them to more complex flow problems. If the physical carbuncle is not properly reproduced, the switching mechanism has to be reworked.

6.2 Influence of viscosity on entropy waves

Some authors consider the carbuncle a result of the treatment of mass transport and entropy waves [40] within the Riemann solver. The hunt for entropy consistent Riemann solvers, e. g., is at least partially driven by that idea. And indeed, for some schemes this causes problems, e. g. for Flux Vector Splitting (FVS) schemes, which may lose positivity by exactly resolving entropy waves [18]. But there is no strict proof, not even the proof by Liou and Steffen in [40], for a connection between the resolution of entropy waves and the carbuncle.

From our considerations in Section 5, we know that the instability of the 1d shock position causes a new Riemann problem perpendicular to the original shock, which includes all types of waves (for gas dynamics also entropy waves). Thus, although the carbuncle occurs also in shallow water, where there are no entropy waves, we can conclude that there is

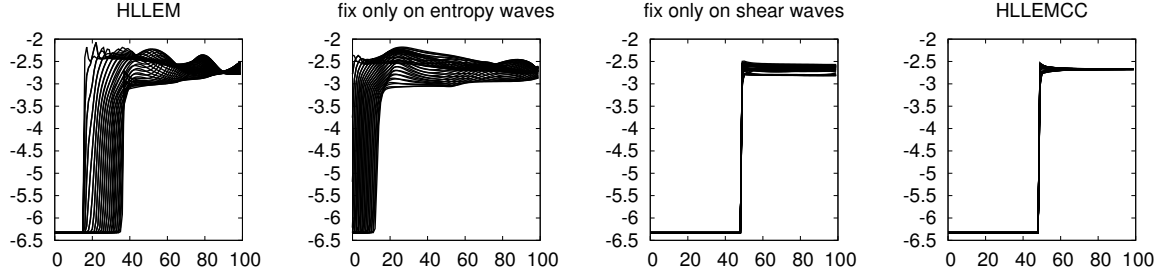


Figure 17: Steady shock in gas dynamics; comparison of HLLM without carbuncle correction, correction on entropy waves, and full HLLMCC at $t = 1000$; entropy shown.

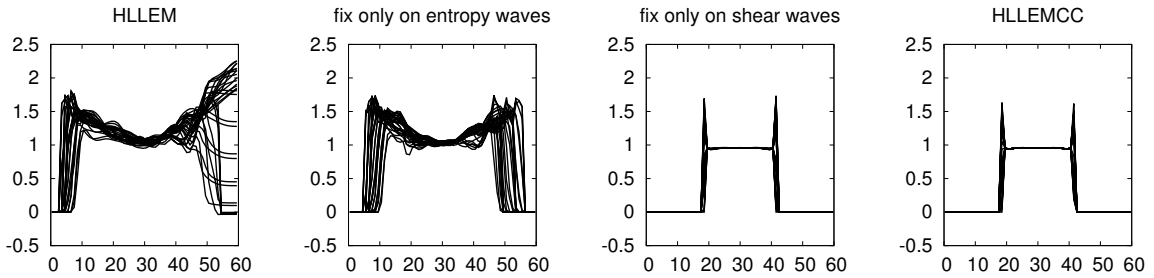


Figure 18: Colliding flow in gas dynamics; comparison of HLLM without carbuncle correction, correction on entropy waves, and full HLLMCC at $t = 20$; entropy shown.

a connection between carbuncle and entropy waves. The question we have to answer is: Which type of waves has the stronger impact on the stability of discrete shock profiles: shear waves or entropy waves?

A good means to answer that question is the HLLMCC solver, which allows to apply the carbuncle correction to both types of linearly degenerate waves separately. In Figures 17 and 18, we present results for the steady shock and the colliding flow problem. We compare pure HLLM with three versions of HLLMCC: correction only applied to entropy waves, correction only applied to shear waves, full HLLMCC. From the numerical results we easily conclude that the resolution of entropy waves contributes to the carbuncle, but the contribution is small compared to the contribution by the shear waves.

7 Conclusions and directions for further research

In this paper, we investigated the origin of the carbuncle phenomenon. Guided by the theoretical results reviewed in Section 3, we found a set of numerical test cases which helped us to sort out the different issues involved in the carbuncle. We observed that the Osher scheme by its special construction of the numerical viscosity on shocks suppresses

the carbuncle to a certain extent. For steady grid-aligned shocks, we could remodel this viscosity in the HLLEM scheme, confirming that it is in fact the numerical viscosity on the shock which is responsible for the stabilizing effect. We also showed how increasing the order offers an alternative way to stabilize the shock position: introducing more degrees of freedom for the scheme allows to remodel the Rankine-Hugoniot condition at a captured shock. This stabilizing mechanism even works when the mechanism of the Osher scheme is not sufficient anymore: in the case of not perfectly-grid aligned shocks like the bow shock in the blunt body problem.

Since the instability of the 1d shock position creates vorticity along the shock, we also considered the influence of the numerical viscosity on entropy and shear waves. We found that the influence of the shear viscosity is much higher than that of the viscosity on entropy waves. We also found (cf. Section 25) that Riemann solvers like HLLEMCC, which try to reduce the carbuncle from within the Riemann solver and without too much loss of the resolution of shear layers, should not be altered when used in a higher order scheme. The gain in stability of the shock position is compensated by the reduction of the shear viscosity. By employing the Elling test we could show that incomplete Riemann solvers like HLLE not only prevent non-physical carbuncles but also the physically induced breakdown of the shock profile when it is hit by a vortex layer.

What is still lacking, is a deeper understanding of the amount of numerical viscosity on shocks in order to stabilize the shock position already for low order schemes. But this would be desirable when one wants to combine the stabilizing mechanisms of Osher and HLLEMCC, in which case the shear viscosity of HLLEMCC could be further reduced. Furthermore, one would hope to be able to extend the theoretical results reviewed in Section 3 to the case of higher order schemes. As we have seen, there is a significant impact of the order of the scheme on the stability of discrete shock profiles.

Acknowledgements

This work was funded by Deutsche Forschungsgemeinschaft (DFG, KE 1420/3-1).

References

- [1] Mohit Arora and Philip L. Roe, *On postshock oscillations due to shock capturing schemes in unsteady flows*, Journal of Computational Physics **130** (1997), 25–40.
- [2] Robert Artebrant and H.Joachim Schroll, *Limit-free third order logarithmic reconstruction.*, SIAM J. Sci. Comput. **28** (2006), no. 1, 359–381 (English).
- [3] Georg Bader and Friedemann Kemm, *The carbuncle phenomenon in shallow water simulations*, The 2nd International Conference on Computational Science and Engineering (ICCSE-2014) (Ho Chi Minh City, Vietnam), 2014.

- [4] Timothy J. Barth, *Some notes on shock resolving flux functions. part 1: Stationary characteristics*, NASA Technical Memorandum 101087, 1989.
- [5] Gabi Ben-Dor, *Shock wave reflection phenomena. 2nd ed.*, Shock Wave and High Pressure Phenomena. Berlin: Springer. xiii, 342 p., 2007.
- [6] A. Bonfiglioli, M. Grottafiume, R. Paciorri, and F. Sabetta, *An unstructured, three-dimensional, shock-fitting solver for hypersonic flows*, *Computers & Fluids* **73** (2013), 162–174.
- [7] Matthieu Bultelle, Magali Grassin, and Denis Serre, *Unstable Godunov discrete profiles for steady waves*, *SIAM Journal on Numerical Analysis* **35** (1998), no. 6, 2272–2297.
- [8] Miroslav Čada and Manuel Torrilhon, *Compact third-order limiter functions for finite volume methods.*, *J. Comput. Phys.* **228** (2009), no. 11, 4118–4145 (English).
- [9] Y. Chauvat, Jean-Marc Moschetta, and Jérémie Gressier, *Shock wave numerical structure and the carbuncle phenomenon*, *International Journal for Numerical Methods in Fluids* **47** (2005), 903–909.
- [10] *Clawpack (conservation laws package)*, <http://www.amath.washington.edu/claw>.
- [11] Tom de Neef and Gino Moretti, *Shock fitting for everybody.*, *Comput. Fluids* **8** (1980), 327–334.
- [12] Michael Dumbser, Jean-Marc Moschetta, and Jérémie Gressier, *A matrix stability analysis of the carbuncle phenomenon*, *Journal of Computational Physics* **197** (2004), 647–670.
- [13] Bernd Einfeldt, *On Godunov-type methods for gas dynamics.*, *SIAM J. Numer. Anal.* **25** (1988), no. 2, 294–318 (English).
- [14] Volker Elling, *The carbuncle phenomenon is incurable*, *Acta Mathematica Scientia* **29** (2009), no. 6, 1647–1656.
- [15] Bjorn Engquist and Stanley Osher, *Stable and entropy satisfying approximations for transonic flow calculations.*, *Math. Comput.* **34** (1980), 45–75.
- [16] Edwige Godlewski and Pierre-Arnaud Raviart, *Hyperbolic systems of conservation laws.*, Paris: Ellipses, 1991.
- [17] ———, *Numerical approximation of hyperbolic systems of conservation laws.*, New York, NY: Springer, 1996.
- [18] Jérémie Gressier, Philippe Villedieu, and Jean-Marc Moschetta, *Positivity of flux vector splitting schemes.*, *J. Comput. Phys.* **155** (1999), no. 1, 199–220 (English).

- [19] L. G. Gvozdeva, O. A. Predvoditeleva, and V. P. Fokeev, *Double mach reflection of strong shock waves*, *Fluid Dynamics* **3** (1968), no. 1, 6—11.
- [20] Amiram Harten and James M. Hyman, *Self adjusting grid methods for one-dimensional hyperbolic conservation laws*, *J. Comput. Phys.* **50** (1983), no. 2, 235–269.
- [21] Amiram Harten, Peter D. Lax, and Bram Van Leer, *On upstream differencing and Godunov-type schemes for hyperbolic conservation laws*, *SIAM Rev.* **25** (1983), no. 1, 35–61.
- [22] P.W. Hemker and S.P. Spekreijse, *Multiple grid and Osher’s scheme for the efficient solution of the steady Euler equations.*, *Appl. Numer. Math.* **2** (1986), 475–493.
- [23] Shi Jin and Jian-Guo Liu, *The effects of numerical viscosities i: Slowly moving shocks*, *Journal of Computational Physics* **126** (1996), 373–389.
- [24] Iraj M. Kalkhoran and Michael K. Smart, *Aspects of shock wave-induced vortex breakdown*, *Progress in Aerospace Sciences* **36** (2000), no. 1, 63–95.
- [25] Friedemann Kemm, *A carbuncle free Roe-type solver for the Euler equations.*, Benzoni-Gavage, Sylvie (ed.) et al., *Hyperbolic problems. Theory, numerics and applications. Proceedings of the 11th international conference on hyperbolic problems*, Ecole Normale Supérieure, Lyon, France, July 17–21, 2006. Berlin: Springer, 2008, pp. 601–608.
- [26] ———, *A comparative study of TVD limiters – well known limiters and an introduction of new ones*, *Internat. J. Numer. Methods Fluids* **67** (2011), no. 4, 404–440.
- [27] ———, *Cfl-number-dependent TVD-limiters*, *Numerical Methods for Hyperbolic Equations: Theory and Applications* (Elena Vázquez-Cendón, Arturo Hidalgo, Pilar García-Navarro, and Luis Cea, eds.), CRC Press, 2012, *Proceedings of the international conference on Numerical Methods for Hyperbolic Equations: Theory and Applications*, Santiago de Compostela, Spain, 4–9 July 2011, pp. 277–283.
- [28] ———, *Contributions to the numerical simulation of gas, shallow water, and plasma flows – wave-wise treatment of order and viscosity*, *Habilitationsschrift*, Brandenburgische Technische Universität, 2014.
- [29] ———, *A note on the carbuncle phenomenon in shallow water simulations*, *ZAMM - Journal of Applied Mathematics and Mechanics / Zeitschrift für Angewandte Mathematik und Mechanik* **94** (2014), no. 6, 516–521.
- [30] ———, *On the proper setup of the double Mach reflection as a test case for the resolution of gas dynamics codes*, *Computers & Fluids* **132** (2016), 72–75.

- [31] Sung-Soo Kim, Chongam Kim, Oh-Hyun Rho, and Seung Kyu Hong, *Cures for the shock instability: Development of a shock-stable roe scheme*, Journal of Computational Physics **185** (2003), 342–374.
- [32] Keiichi Kitamura, *A further survey of shock capturing methods on hypersonic heating issues*, AIAA Paper **2698** (2013).
- [33] Keiichi Kitamura, Philip Roe, and Farzad Ismail, *Evaluation of euler fluxes for hypersonic flow computations*, AIAA Journal **47** (2009), no. 1, 44–53.
- [34] Keiichi Kitamura, Eiji Shima, Yoshiaki Nakamura, and Philip L Roe, *Evaluation of euler fluxes for hypersonic heating computations*, AIAA journal **48** (2010), no. 4, 763–776.
- [35] Culbert B. Laney, *Computational gasdynamics.*, Cambridge: Cambridge University Press, 1998.
- [36] Randall J. LeVeque, *Numerical methods for conservation laws. 2nd ed.*, Basel: Birkhäuser. x, 214 p. , 1992 (English).
- [37] Randall J. Leveque, *Finite volume methods for hyperbolic problems.*, Cambridge Texts in Applied Mathematics. Cambridge: Cambridge University Press, 2002 (English).
- [38] Randall J. LeVeque, Dimitri Mihalas, E. A. Dorfi, and Ewald Müller, *Computational methods for astrophysical fluid flow*, Springer, Berlin, Heidelberg, 1998.
- [39] H. Li and G. Ben-Dor, *A shock dynamics theory based analytical solution of double Mach reflections.*, Shock Waves **5** (1995), no. 4, 259–264.
- [40] Meng-Sing Liou and Christopher J. Steffen, *A new flux splitting scheme.*, J. Comput. Phys. **107** (1993), no. 1, 23–39 (English).
- [41] G. Moretti and M. Abbett, *A time-dependent computational method for blunt body flows.*, AIAA J. **4** (1966), 2136–2141.
- [42] Gino Moretti, *Thirty-six years of shock fitting.*, Comput. Fluids **31** (2002), no. 4-7, 719–723.
- [43] J.-M. Moschetta, J. Gressier, J.-C. Robinet, and G. Casalis, *The carbuncle phenomenon: a genuine Euler instability?*, Toro, E. F. (ed.), Godunov methods. Theory and applications. International conference, Oxford, GB, October 1999. New York, NY: Kluwer Academic/Plenum Publishers. 639-645 (2001)., 2001.
- [44] Stanley Osher and Fred Solomon, *Upwind difference schemes for hyperbolic systems of conservation laws.*, Math. Comput. **38** (1982), 339–374.

- [45] Maurizio Pandolfi and Domenic D' Ambrosio, *Numerical instabilities in upwind methods: Analysis and cures for the carbuncle phenomenon*, Journal of Computational Physics **166** (2001), no. 2, 271–301.
- [46] Soo Hyung Park and Jang Hyuk Kwon, *On the dissipation mechanism of Godunov type schemes*, Journal of Computational Physics **188** (2003), 524–542.
- [47] KM Peery and ST Imlay, *Blunt-body flow simulations*, AIAA, SAE, ASME, and ASEE, Joint Propulsion Conference, 24 th, Boston, MA, 1988.
- [48] James J. Quirk, *A contribution to the great Riemann solver debate*, International Journal for Numerical Methods in Fluids **18** (1994), 555–574.
- [49] Jean-Christophe Robinet, Jérémie Gressier, G. Casalis, and Jean-Marc Moschetta, *Shock wave instability and the carbuncle phenomenon: Same intrinsic origin?*, Journal of Fluid Mechanics **417** (2000), 237–263.
- [50] Philip L. Roe, *Approximate riemann solvers, parameter vectors, and difference schemes*, J. Comput. Phys. **43** (1981), no. 2, 357–372.
- [51] PL. Roe and M.J. Baines, *Algorithms for advection and shock problems.*, Numerical methods in fluid mechanics, Proc. 4th GAMM-Conf., Paris 1981, Notes Numer. Fluid Mech. 5, 281-290 (1982)., 1982.
- [52] Manuel D. Salas, *A shock-fitting primer. With CD-ROM.*, Boca Raton, FL: CRC Press, 2010 (English).
- [53] Richard Sanders, Eric Morano, and Marie-Claude Druguet, *Multidimensional dissipation for upwind schemes: Stability and applications to gas dynamics*, Journal of Computational Physics **145** (1998), no. 2, 511–537.
- [54] Lewis B. Schiff and Joseph L. Steger, *Numerical simulation of steady supersonic viscous flow*, AIAA Journal **18** (1980), 1421–1430.
- [55] Susana Serna and Antonio Marquina, *Power ENO methods: A fifth-order accurate weighted power ENO method.*, J. Comput. Phys. **194** (2004), no. 2, 632–658 (English).
- [56] Joseph L. Steger and R.F. Warming, *Flux vector splitting of the inviscid gasdynamic equations with application to finite-difference methods.*, J. Comput. Phys. **40** (1981), 263–293 (English).
- [57] E. F. Toro, M. Spruce, and W. Speares, *Restoration of the contact surface in the hll-riemann solver*, Shock Waves **4** (1994), no. 1, 25–34.
- [58] Eleuterio F. Toro, *Riemann solvers and numerical methods for fluid dynamics. A practical introduction. 3rd ed.*, Berlin: Springer, 2009 (English).

- [59] Guohua Tu, Xiaohui Zhao, Meiliang Mao, Jianqiang Chen, Xiaogang Deng, and Huayong Liu, *Evaluation of Euler fluxes by a high-order cfd scheme: shock instability*, International Journal of Computational Fluid Dynamics **28** (2014), no. 5, 171–186.
- [60] Bram van Leer, *Towards the ultimate conservative difference scheme. IV: A new approach to numerical convection.*, J. comput. Phys. **23** (1977), 276–299 (English).
- [61] Pieter Wesseling, *Principles of computational fluid dynamics.*, Berlin: Springer, 2000.
- [62] Paul Woodward and Phillip Colella, *The numerical simulation of two-dimensional fluid flow with strong shocks.*, J. Comput. Phys. **54** (1984), 115–173.
- [63] D. W. Zaide and P. L. Roe, *Flux functions for reducing numerical shockwave anomalies*, sign **1** (2012), 2.
- [64] Daniel W. Zaide and Philip L. Roe, *Shock capturing anomalies and the jump conditions in one dimension*, 20th AIAA CFD Conference, 2011.
- [65] Daniel Wei-Ming Zaide, *Numerical shockwave anomalies*, Ph.D. thesis, The University of Michigan, 2012.
- [66] Shuhai Zhang, Hanxin Zhang, and Chi-Wang Shu, *Topological structure of shock induced vortex breakdown*, Journal of Fluid Mechanics **639** (2009), 343–372.